Applied Catalysis B: Environmental 256 (2019) 117859

Contents lists available at ScienceDirect

Applied Catalysis B: Environmental

journal homepage: www.elsevier.com/locate/apcatb

Alkali-metal poisoning effect of total CO and propane oxidation over Co_3O_4 nanocatalysts

Wenxiang Tang[a], Junfei Weng[a], Xingxu Lu[a], Liaoyong Wen[a], Ashwanth Suburamanian[b], Chang-Yong Nam[b,c], Pu-Xian Gao[a,*]

[a] Department of Materials Science and Engineering & Institute of Materials Science, University of Connecticut, 97 North Eagleville Road, Storrs, CT, 06269-3136, USA
[b] Department of Materials Science and Chemical Engineering, Stony Brook University, Stony Brook, NY, 11974, USA
[c] Center for Functional Nanomaterials, Brookhaven National Laboratory, Upton, NY, 11973, USA

ARTICLE INFO

Keywords:
: Cobalt oxide
Alkali metals
Poisoning effect
Catalytic oxidations

ABSTRACT

Cobalt oxide (Co_3O_4), a low-cost transitional metal oxide, has been widely studied for catalytic total oxidation of CO and hydrocarbons. However, much less attention has been paid to the poisoning effect due to alkali metals in such oxidation catalysts despite the ease of access to such poisons in both mobile and stationary combustion sources. In this study, the alkali metals such as Na, K and Li were readily deposited onto a Co_3O_4 catalyst to study their poisoning effect on CO and propane oxidation. 1% doping onto Co_3O_4 was found to increase the light-off temperature by 50 °C in CO oxidation and over 160 °C in propane oxidation. It is also noted that alkali metals exhibited a 'locking-effect' on oxygen of Co_3O_4, leading to poor oxygen mobility of alkali metal doped catalysts. During the reaction, alkali metals can significantly promote the adsorption of CO_2 to form robust surface carbonate species even at high temperature, another reason for the poisoning effect of alkali metals on Co_3O_4 nanocatalysts for catalytic oxidation.

1. Introduction

Over the past few decades, thermal catalytic oxidation with high efficiency at low operating temperature has been considered as an effective technique for elimination various combustion induced pollutants such as CO, hydrocarbons (HCs), and carbonaceous soot particles [1–3]. The research and development of high-activity catalysts plays a key role for the broad application of oxidation catalysts. Supported noble metal catalysts have been widely implemented for a broad array of oxidative reactions, as applied in many practical exhaust aftertreatment devices such as three-way catalyst (TWC) and diesel oxidation catalyst (DOC) for oxidation of CO and hydrocarbons. However, such industrial applications of these catalysts are limited due to their disadvantages such as high price, low thermal stability, sintering and poisoning tendency [4–6]. On the other hand, low-cost transition metal oxides have been proved to be active in CO and hydrocarbons oxidations at low temperature, therefore holding promises in practical applications [2,7,8].

Co_3O_4, a typical transition metal oxide with a spinel crystal structure, has been extensively reported as effective catalysts for CO/NO/HCs oxidations, soot combustion, selective catalytic reduction of NO_x, N_2O decomposition, water splitting *etc*. [9–16]. For example, Xie et al. reported the Co_3O_4 nanorods can catalyze CO oxidation at temperatures as low as −77 °C and remain stable in a moist stream of normal feed gases [17]. Moreover, Co_3O_4 is also highly active for hydrocarbon combustion under condition of low temperature and low hydrocarbon concentrations [10,18,19]. Unlike noble metal catalysts, Co_3O_4 based catalyst can keep high activity for hydrocarbon oxidation even with CO as a co-feed gas [20]. But challenges remain such as the poisoning effect of sulfur-containing species, thermal stability, and water inhibition. Many attentions have been paid on improving its performance by novel nanostructuring, transition metal doping, low-cost supports, and low-usage of noble metals [10,12,18,20–26], but few studies have been devoted to the poisoning effect of alkali metals on Co_3O_4 catalyst. In fact, alkali metals widely exist in the exhaust of coal-fired plants and municipal solid waste incineration plants, a major concern for selective catalytic reduction (SCR) catalysts due to their reactivity with active sites [27]. In addition, alkali metals can be found in vehicle exhaust as originated from fuel/oil additives and urea solutions for SCR operation [27,28]. Usually existed as a common compound in various exhausts, alkali metal might be a great concern for an aftertreatment system that adopts low-cost transition metal oxides such as Co_3O_4 as a catalyst. Moreover, nanostructured Co_3O_4 based catalysts have been made using conventional alkali metal salts such as NaOH and Na_2CO_3 as

* Corresponding author.
E-mail address: puxian.gao@uconn.edu (P.-X. Gao).

https://doi.org/10.1016/j.apcatb.2019.117859
Received 21 January 2019; Received in revised form 17 April 2019; Accepted 9 June 2019

precipitants [24,26,29], while the potential contamination effect due to alkali metals has been ignored to a great extent.

In general, the catalysts could be deactivated by poisons such as sulfur, heavy metals, alkali metals, fly ashes in the emitted gas through chemical deactivation or pore blocking. Like SCR process, deposition of alkali and alkaline earth metal salts in fly ashes can significantly deactivate the typical V_2O_5 based catalysts like V_2O_5–WO_3/TiO_2 [30], V_2O_5/CeO_2 [31] and V_2O_5/TiO_2 [32], which has become one of the main problems for practical applications. Several alkali poisoning mechanisms have been proposed so far. First, Na^+ ions are suggested to combine strongly with dispersed vanadia species and neutralize the Brønsted acid sites which will decrease surface acidity and further suppress NH_3 adsorption. Secondly, alkali metals can also reduce the catalyst reducibility that prohibits NH_3 activation and NO oxidation by forming bonding of alkali to active vanadia or ceria. Thirdly, the formation of inactive nitrate species will be promoted by creation of new basic sites. On the contrary, alkali metals sometime can have promoting effect in specific catalytic reaction systems. For example, Na^+ ions have been proved to improve the dispersion of noble metal (*e.g.*, Pt and Pd) on metal oxide support by forming atomically dispersed Na-Pt-$O(OH)_x$ species, which can effectively activate H_2O and catalyze the facile reaction between surface OH^- and formate species to total oxidation products, further enhance the catalytic activities in formaldehyde oxidation [33]. Another important reaction is catalytic combustion of soot, where the alkali metal itself can involve the oxidative process through formation of carbon–oxygen complexes (C–O–M, with M alkali metals) as the active sites and further enhance the activity of soot oxidation [34,35]. For non-precious metal oxides, very few studies have been focused on the effect of alkali metal on their activities in CO and hydrocarbon oxidation despite the fact that alkali metals are popular components in different gas emissions. Hutchings et al. [36] found the ageing of copper manganese oxide catalysts could lead to a significant decrease in the concentration of surface sodium and further improve its activity in CO oxidation. Nevertheless, the effect of alkali metals on catalytic reactions over different catalysts could be totally different. Herein, this study systematically investigates for the first time the poisoning effect of Co_3O_4 catalyst in CO and hydrocarbons (C_3H_8,C_3H_6 and CH_4) oxidation by alkali metals including Na, K and Li. These alkali metals have displayed significant poisoning effects for both CO and propane oxidations. XRD, SEM and TEM studies show that alkali metal doping does not affect the crystal structure and morphology of Co_3O_4 catalyst. O_2-TPD results confirm the 'locking-effect' of alkali metals where the mobility of oxygen species is significantly inhibited with alkali metals doping especially at low temperature. Moreover, in-situ DRIFTS studies show alkali metals can significantly promote the adsorption of CO_2 to form robust surface carbonate species even at high temperature (> 380 °C), which might be another reason for the poisoning effect of alkali metals on Co_3O_4 nanocatalysts for catalytic oxidation.

2. Materials and methods

2.1. Materials preparation

2.1.1. Synthesis of Co_3O_4 nanoparticles

An oxalate-precipitation method was applied to prepare the cobalt oxalate precursor in an alcoholic solution, which was further dried and annealed under atmosphere to get the Co_3O_4 nanoparticles catalyst. Typically, 100 ml solution A containing 20 mmol $Co(NO_3)_2$ and another 100 ml solution B containing 24 mmol oxalic acid were mixed at room temperature and the precipitation reaction occurred in a few seconds. After strongly stirring for 30 min, the mixture was directly dried at 80 °C for 48 h. Finally, the precipitate was treated at 500 °C for 2 h with a ramp rate of 5 °C min^{-1} in a muffle furnace to get fresh Co_3O_4 nanoparticles which were further used for deposition of alkali metals.

2.1.2. Deposition of alkali metals on Co_3O_4

Traditional impregnation method was adopted for depositing alkali metals on the as-prepared Co_3O_4 nanocatalyst. In a typical process, the fresh Co_3O_4 powder was immersed into a solution with certain amount of $NaNO_3$, then the mixture was ultrasonically treated for 30 min and further dried at 80 °C, finally annealed at 450 °C for 2 h with a ramp rate of 5 °C min^{-1} in a muffle furnace. The weight-based loading ratios of Na were about 0%, 1%, 2%, 5%, and the related samples were denoted as Co_3O_4, 1% Na-Co_3O_4, 2% Na-Co_3O_4 and 5% Na-Co_3O_4, respectively. Moreover, other two alkali metals (K and Li, with KNO_3 and $LiNO_3$ respectively) deposition were also prepared by same process with 1% loading ratio, and the final materials were named as 1% K-Co_3O_4 and 1% Li-Co_3O_4, respectively.

2.2. Materials characterization

The X-ray diffraction (XRD) patterns of the as-prepared catalysts were achieved by an X-ray diffractometer (D2 PHASER, BRUKER Corp.) with a 2θ scan rate of 10° min^{-1}. Scanning electron microscopy (SEM, Teneo LVSEM, FEI) and transmission electron microscopy (TEM, Talos S/TEM, FEI; 200 kV acceleration voltage) were applied to get the morphology and microstructure of the as-prepared catalysts. A surface analyzer (ASAP 2020, Micromeritics Corp.) was used to do the N_2 adsorption-desorption testing and the surface area was obtained according to the Brunauer-Emmett-Teller (BET) method. For each measurement, a degassing process was carried out at 150 °C for 6 h. Oxygen temperature programmed desorption (O_2-TPD) were carried out in a U-shaped quartz reactor under a gas flow of pure Ar (25 ml min^{-1}) on a Chemisorption system (ChemiSorb 2720, Micromeritics Cor.). Before doing the O_2-TPD analysis, 30 mg sample was loaded and pretreated under oxygen atmosphere at 250 °C for 1 h and cooled down to 50 °C then purged with pure argon gas for a few hours. In every run, the temperature was ramped to 800 °C from 50 °C at a rate of 10 °C min^{-1}. NH_3-TPD procedure is similar to O_2-TPD analysis while the adsorption gas was changed to NH_3 and a mass spectrometer (Hiden HPR-20) was used for detecting NH_3 concentration with signal of m/z = 17. The CO_2-TPD procedure is similar to O_2-TPD analysis while the adsorption gas was changed to 20% CO_2 in Ar and a mass spectrometer (Hiden HPR-20) was used for monitoring CO_2 concentration with signal of m/z = 44. CO temperature programmed reduction (CO-TPR) were carried out in a quartz tube reactor under a gas flow of 5% CO balanced with Ar, and the concentration of both CO and CO_2 were detected by Micor-GC (Agilent 490). In each run, the temperature was ramped to 750 °C from 50 °C at a rate of 5 °C min^{-1}. The infrared tests were carried out on a Fourier Transform Infrared Spectrophotometer (Nicolet iS-50 FTIR Spectrometer, Thermo Scientific). The tested powders were 1–2 mg prepared catalyst sample mixed with 100 mg KBr which was filled in the sample cell on the spectrophotometer and further pressed appropriately. The infrared spectrum was recorded in the region 600–4000 cm^{-1} with 64 scans at resolution of 4 cm^{-1}.

In situ diffuse reflectance infrared spectroscopy (DRIFTS) study was also performed on the same spectrometer equipped with an MCT detector cooled by liquid nitrogen. Typically, the sample powder (25 mg) was mixed with 100 mg KBr treated *in situ* at 250 °C in 10% O_2/N_2 with a flow rate of 50 ml min^{-1} to eliminate surface contaminants. After the system was cooled to 30 °C, a background spectrum was collected for spectra correction. Then, 2500 ppm CO (or 2500 ppm C_3H_8), 10% O_2 in N_2 with a flow rate of 50 ml min^{-1} was introduced to the in-situ chamber while the temperature of chamber is ramping to 300 °C (or 400 °C with a rate of 2 °C min^{-1} when doing propane oxidation). The related spectra were collected at different temperature, accumulating 32 scans at a resolution of 2 cm^{-1} and displayed in Kubelka-Munk units.

2.3. Catalytic performance test

Two classic probe oxidation reactions including CO and propane oxidation were adopted to investigate the poisoning effect of alkali metals on cobalt oxide catalyst. A home-made plug flow reactor was used to test the oxidation reactions of CO and propane by the prepared catalysts, with the inlet and outlet gaseous species detected by a gas chromatography system (Agilent Micro-GC 490) equipped with three columns (two molecular sieve columns and one Plot-Q column) and three thermal conductivity detectors (TCD). The reactant gas was 2500 ppm CO (or 2500 ppm C_3H_8), 10% O_2 and 89.75% N_2 with a total flow rate of 100 ml min^{-1}. 50 mg catalyst powder mixed with 200 mg quartz sands (40–80 mesh) was placed into the center of quartz tube (1/4 in. diameter) and pressed from both sides with quartz wool. A thermocouple wire was inserted into the reactor for measuring the catalyst bed temperature. With this condition, the catalyst weight-hourly space velocity could be controlled at 120,000 ml $g^{-1} h^{-1}$. In order to investigate the effect of $H_2O/CO_2/SO_2$ on the catalysts in C_3H_8 combustion, the final concentration of H_2O, CO_2 and SO_2 were controlled at 3%, 8% and 10 ppm, respectively, for the test, while keeping other condition constant. Moreover, two other hydrocarbons (C_3H_6 and CH_4) were also applied in the test, with their concentrations maintained at 2500 ppm.

3. Results and discussion

3.1. Poisoning effect on catalytic oxidations

Fig. 1 displays the CO and propane oxidation activities of pure Co_3O_4 and alkali metal doped Co_3O_4 catalysts tested from a ramping process from 50 to 420 °C (2 °C min^{-1}) under a WHSV of 120,000 ml $g^{-1} h^{-1}$. The T_{10}, T_{50} and T_{90} values (the reaction temperature corresponding to the CO or C_3H_8 conversion of 10%, 50% and 90%, respectively) were used to compare the activities as-prepared catalysts, and the results are listed in Table 1. As shown in Fig. 1a, over the pure Co_3O_4 nanocatalysts, the values of T_{10}, T_{50} and T_{90} are 63, 90, 107 °C, respectively, while they are 110, 110, 160 °C over 1% Na doped Co_3O_4, respectively. As we can see, the doped Na has significant poisoning effect on CO oxidation of Co_3O_4. With increasing the doping amount from 1% to 5%, the T_{90} was obviously delayed from 160 °C to 259 °C, which is 148 °C higher than the undoped Co_3O_4. Therefore, the extent of deactivation is highly depended on the doped concentration of the poisoning metals which means more Na doping will have more poisoning effect on the CO oxidation activity of Co_3O_4. Compared to CO oxidation, the poisoning effect of Na on propane oxidation is more evident as revealed in Fig. 1b. The values of T_{10}, T_{50} and T_{90} for propane oxidation on undoped Co_3O_4 are 207, 225, 241 °C, respectively, while the conversion is only 32% at 400 °C over 1% Na doped Co_3O_4. Similarly, the poisoning effect becomes more serious with developing amount of Na doping. Moreover, the poisoning effect of different alkali metals on oxidation activities of Co_3O_4 was also investigated as shown in Fig. 1c and d. n. For both CO and propane oxidation, the light-off temperature shifts to higher level in the order of Li < K < Na with same loading ratio of 1%. With these findings, it clearly indicates that the Co_3O_4 catalyst can be seriously poisoned by alkali metals during the CO and hydrocarbon combustions, so the practical oxidation applications of Co_3O_4 nanocatalyst should avoid the exhaust condition with alkali metals.

In order to investigate the effect of different alkali metal source on the activity of Co_3O_4, several Na based salts like NaCl, $NaCH_3COO$ and $Na_3C_6H_5O_7$ were selected for Na loading, and the results are shown in Fig. 2. It can be seen all Na doped samples with different Na source can poison the activities in both CO and propane oxidation, where the poisoning effect of NaCl-derived catalyst is the weakest one. Considering the properties of Na salts, NaCl is difficult to decompose within the treating temperature we used in this study so that the doping effect will not be fully achieved. In addition, some other components like $H_2O/CO_2/SO_2$ which could be usually found in realistic combustion gas conditions may have potential poisoning effects on the related catalytic reactions. In this case, 3.0% water or 8% CO_2 or 10 ppm SO_2 was introduced in the propane oxidation reaction, and the results are shown in Fig. 3. For the pure Co_3O_4 catalyst, H_2O and CO_2 have slight effect on

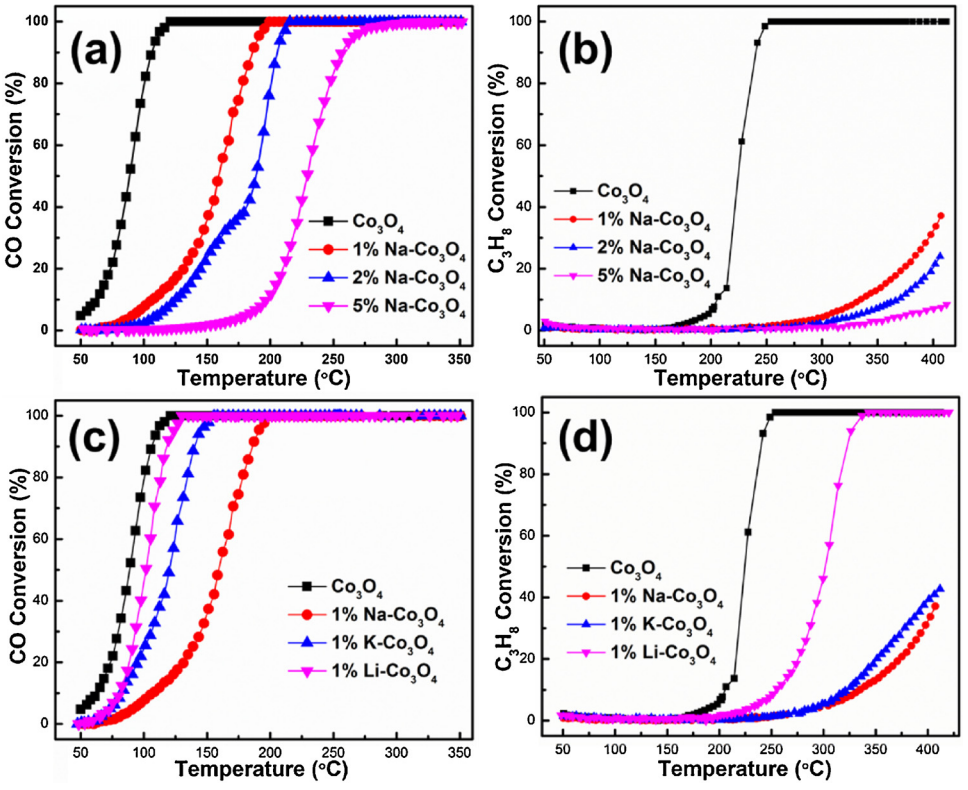

Fig. 1. Comparison of oxidation activities of pure Co_3O_4 and alkali metal doped Co_3O_4 catalysts. (a) and (b) CO and propane oxidation over Na doped Co_3O_4 with different doping ratios. (c) and (d) CO and propane oxidation over pure, 1% Na, 1% K and 1% Li doped Co_3O_4. Reaction conditions: catalyst 50 mg, [CO] = 2500 ppm or [C_3H_8] = 2500 ppm, [O_2] = 10%, flow rate = 100 ml min^{-1}, WHSV = 120,000 ml $g^{-1} h^{-1}$.

Table 1
Catalytic activities (temperature of 10% (T10), 50% (T50) and 90% (T90) conversion), crystal size (calculated by XRD patterns) and BET surface area of pure Co_3O_4 and alkali metal doped Co_3O_4 catalysts.

Catalyst	Catalytic CO oxidation			Catalytic propane oxidation			Crystal size(nm)	BET surface area ($m^2 g^{-1}$)
	T10 (°C)	T50 (°C)	T90 (°C)	T10 (°C)	T50 (°C)	T90 (°C)		
Co_3O_4	63	90	107	207	225	241	35.3	14.2
1%Na-Co_3O_4	110	110	160	336	> 400	> 400	35.3	14.8
2%Na-Co_3O_4	127	128	189	367	> 400	> 400	35.2	13.7
5%Na-Co_3O_4	200	230	259	> 400	> 400	> 400	35.3	15.1
1%K-Co_3O_4	82	121	140	325	> 400	> 400	35.2	13.8
1%Li-Co_3O_4	82	102	118	254	302	325	35.2	14.5

the light-off activity of propane oxidation and the complete converted temperature delay is below 20 °C, while SO_2 has a seriously negative effect on the propane oxidation and the total oxidation temperature is 150 °C higher than that of pure one. Over the Na doped Co_3O_4 catalyst, all introduced components show negative effect on the propane oxidation activity, which are more serious than the undoped Co_3O_4. It is a remarkable fact that the effect of CO_2 on the activity of Na doped Co_3O_4 catalyst is even worse than SO_2, indicating the doped Na on the catalyst has certain connection with the gaseous CO_2 or surface carbonate species. It will be a great challenge for pure Co_3O_4 when applying in the combustion exhaust with both alkali metals and high concentration of CO_2. The possible mechanism will be discussed in the later DRIFT studies. Moreover, similar poisoning effect was also observed when the catalysts were applied in catalytic combustion of other hydrocarbons such as C_3H_6 and CH_4. As displayed in Fig. 4a and b, the light-off curves for both C_3H_6 and CH_4 have been pushed to higher temperature when Co_3O_4 was doped with 1% Na, indicating this poisoning effect due to alkali metal is a common for Co_3O_4 in oxidation reactions. Furthermore, the effect of alkaline metal on catalyst stability study was also studied, and revealed in Fig. 4c. For pure Co_3O_4, the conversion of CO can keep at 100% under 2 testing temperatures (175 and 165 °C). But for 1%Na-Co_3O_4, the conversion of CO at 175 °C decreased dramatically during the first 3 h and then kept stable. However, decreasing temperature to 165 °C, the conversion also decreased dramatically during the first 3 h but then kept reducing throughout the reaction time. Clearly, something changed when the catalyst was exposed to single CO, such as the accumulation of carbonate species (as explained in DRIFT study), which will further deactivate the catalyst for CO oxidation.

3.2. XRD patterns

Fig. 5 displays the wide-angle XRD patterns the pure Co_3O_4 and alkali metal doped Co_3O_4 samples. From pure Co_3O_4, there are only several diffraction peaks at 2θ = 31.2, 36.8, 44.8, 59.2 and 65.1° can be clearly observed, which can be ascribed to the {220}, {311}, {400}, {511} and {440} planes of Co_3O_4 (JCPDS 78–1969). With Na doping, the obtained catalysts keep same crystalline Co_3O_4 with typical spinel type structure and no any other peaks has been observed even with higher Na doping like 5% Na-Co_3O_4. We assume that sodium species are well dispersed on the cobalt oxide surface, which are consistent with other reports [37,38]. For different alkali metals doping, the crystal files are absolutely same, and all catalysts have similar crystal size of about 35.2 nm achieved by Scherrer Equation calculation and also have similar BET surface area as listed in Table 1, further confirming that the doping alkali metals have no effect on the crystal character of original Co_3O_4.

3.3. FTIR spectra

Fig. 6 shows the FTIR spectra of pure Co_3O_4 and alkali metal doped Co_3O_4 catalysts. Over all FTIR spectra of catalysts, the peaks at around 663 and 567 cm^{-1} are ascribed to the Co-O vibrations of the Co_3O_4 [39,40], further confirming the alkali metals doping haven't changed the crystal structure of Co_3O_4. With low doping amount of Na and K (1%), no difference was observed on the FTIR spectra, which suggested that the low doping amount of Na or K has been well dispersed on the matrix of Co_3O_4. When the doping amount of Na increased to 5%, some additional peaks at 831 and 1383 cm^{-1} can be clearly observed compared to the spectra of pure Co_3O_4, which can be assigned to the stretching vibration of CO_3^{2-} species [41,42]. The observance of CO_3^{2-} on higher content of Na doping indicates that the doping Na amount is limited, and the additional Na will turn into some other compounds like Na_2CO_3 by adsorbing the CO_2 from air during the treated procedure. Meanwhile, some different absorption bands 865, 1381, 1435 cm^{-1} can be assigned to the CO_3^{2-} vibration of the Li_2CO_3 [41] or undecomposed nitrate groups [43], and the intensive band at 3435 cm^{-1} belongs to the O–H stretching mode of adsorbed water. All the aforementioned XRD and FTIR results unambiguously reveal that after modification with alkali metals the structure of Co_3O_4 retains with both Na and K dispersed on the Co_3O_4 without any additional Na/K compounds.

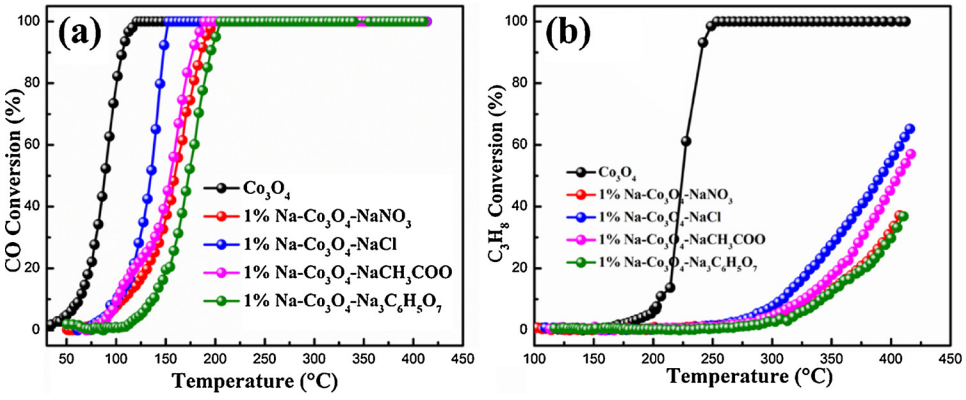

Fig. 2. Comparison of oxidation activities of pure Co_3O_4 and 1%Na doped Co_3O_4 catalysts with using different Na source ($NaNO_3$, NaCl, $NaCH_3COO$, $Na_3C_6H_5O_7$). (a) and (b) CO and propane oxidation. Reaction conditions: catalyst 50 mg, [CO] = 2500 ppm or [C_3H_8] = 2500 ppm, [O_2] = 10%, flow rate = 100 ml min^{-1}, WHSV = 120,000 ml $g^{-1} h^{-1}$.

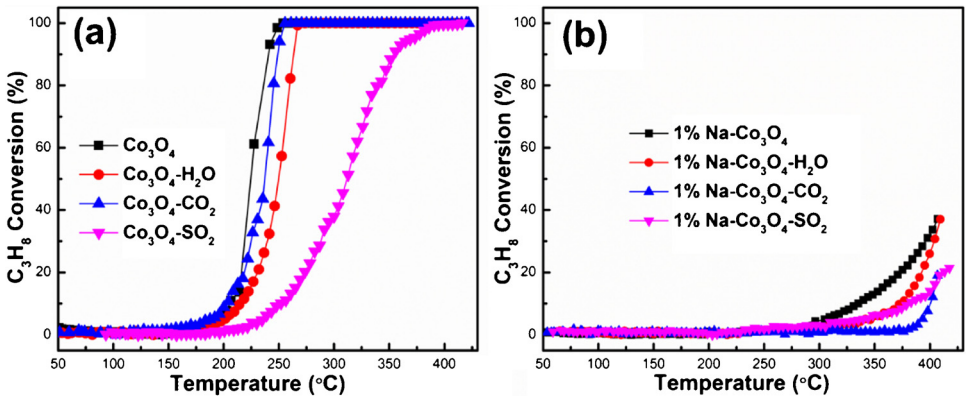

Fig. 3. Comparison of propane oxidation activities of (a) pure Co_3O_4 and (b) 1%Na doped Co_3O_4 catalysts with/without introducing different components. Reaction conditions: catalyst 50 mg, [CO] = 2500 ppm or [C_3H_8] = 2500 ppm, [O_2] = 10%, 3% H_2O or 8% CO_2 or 10 ppm SO_2 flow rate = 100 ml min^{-1}, WHSV = 120,000 ml g^{-1} h^{-1}.

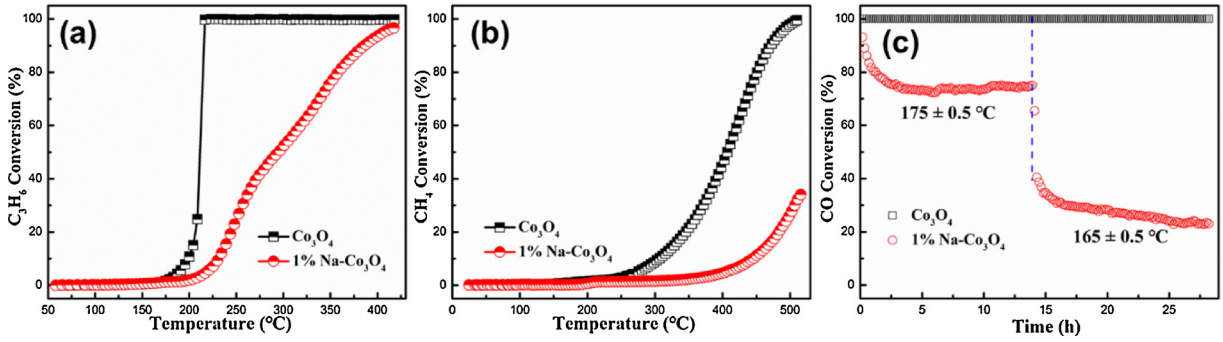

Fig. 4. (a) and (b) Comparison of propylene and methane oxidation activities over pure Co_3O_4 and 1%Na doped Co_3O_4 catalysts. (c) Stability of CO oxidation at 175 and 165 °C over pure Co_3O_4 and 1%Na doped Co_3O_4 catalysts. Reaction conditions: catalyst 50 mg, [C_3H_6] = 2500 ppm or [CH_4] = 2500 ppm or [CO] = 2500 ppm, [O_2] = 10%, flow rate = 100 ml min^{-1}, WHSV = 120,000 ml g^{-1} h^{-1}.

3.4. Morphologies and microstructures

The morphologies of as-prepared catalysts have been revealed by the SEM images in Fig. 7a–f. It can be seen that the pure Co_3O_4 is an aggregate which keeps very well after doping with alkali metals. In TEM images of Fig. 8a–d, the aggregate assembled with irregular polyhedron nanoparticles can be clearly observed, and the average size is about 30–40 nm, in agreement with the value calculated by XRD patterns. For both pure Co_3O_4 and 1% Na doped samples, a lattice spacing of 0.29 nm can be observed on the randomly selected nanoparticles (Fig. 8b and d) that is ascribed to the {220} planes of spinel Co_3O_4 crystals. Furthermore, little change was observed on the morphology and crystal structure of Co_3O_4 after doping with alkali metals. Moreover, the HAADF-STEM imaging and elemental mapping (Fig. 8e–h) confirm the elemental composition distribution of the alkali doped catalysts. The results also demonstrate that Na is homogeneously distributed throughout the whole nanocrystals, suggesting the successful integration of the alkali metal and Co_3O_4 components.

3.5. O_2-TPD, NH_3-TPD, CO_2-TPD, CO-TPR and XPS

Oxygen mobility on metal oxide catalysts plays an important role in oxygen-involved catalytic reactions [26,44–46]. The O_2-TPD technique is a good method to investigate the oxygen mobility of different oxygen species on the catalysts and the results are shown in Fig. 9. Generally, the oxygen species on Co_3O_4 can be classified as surface adsorbed oxygen species, surface lattice oxygen and bulk lattice oxygen. Considering the thermodynamics of Co_3O_4, the decomposition of Co_3O_4 to form CoO only takes place above 900 °C [47], which can be assigned to the desorption of bulk lattice oxygen. Meanwhile, the desorption of surface adsorbed oxygen species and surface lattice oxygen can proceed at lower temperature which are expected to be the active species during

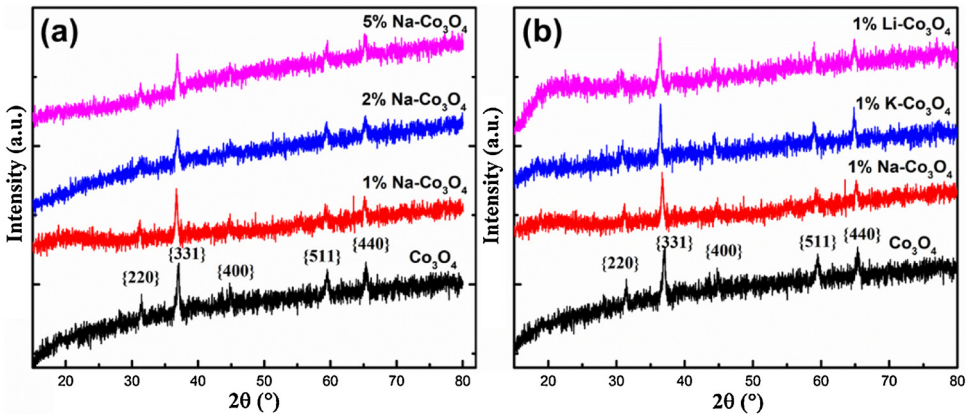

Fig. 5. XRD patterns of pure Co_3O_4 and alkali metal doped Co_3O_4 catalysts.

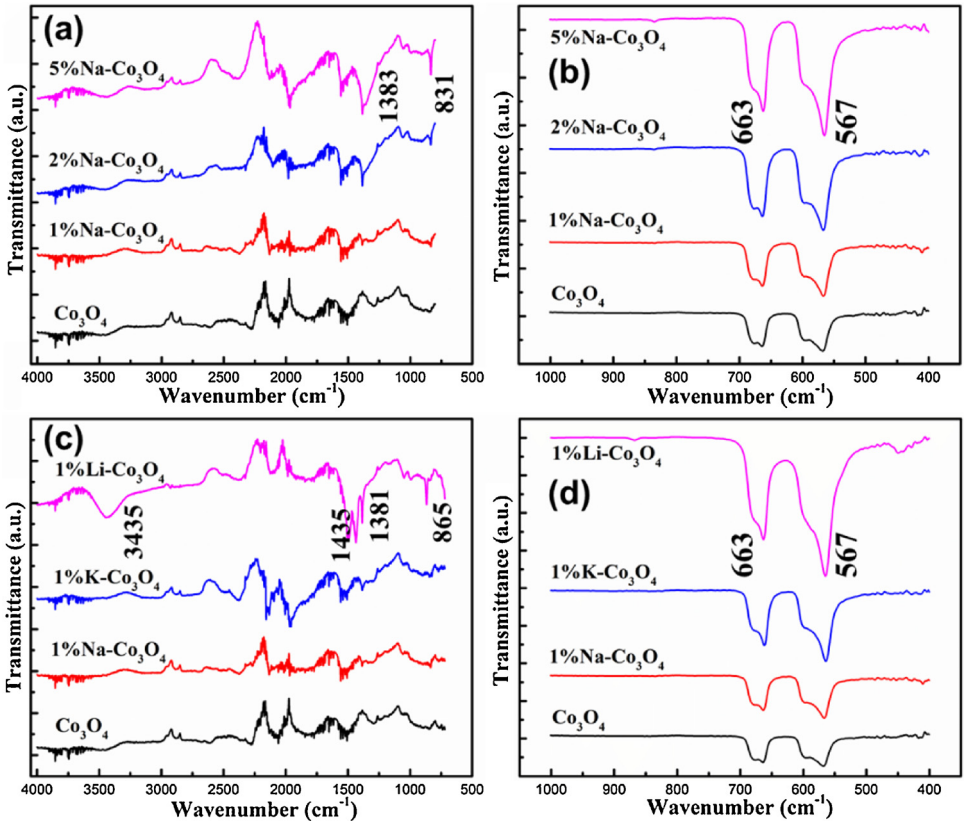

Fig. 6. FTIR spectra of pure Co_3O_4 and alkali metal doped Co_3O_4 catalysts.

the catalytic oxidation species [9,21,22,26,45,46,48] due to their nature of easy regeneration in oxidized atmosphere. For O_2-TPD of pure Co_3O_4 displayed in Fig. 9a, one peak below 250 °C and another peak around 250–450 °C can be assigned to the desorption of surface adsorbed oxygen species and surface lattice oxygen species, respectively [49,50]. With 1% Na doping, the desorption peak below 200 °C almost disappears and two other broad peaks can be observed at higher temperature, demonstrating that the oxygen mobility has been significantly affected and the utilization of surface oxygen species becomes difficult. Furthermore, the desorption peaks move to higher temperature when increasing the doping amount of sodium, further confirming the "locking-effect" of sodium on surface active oxygen species of Co_3O_4 catalyst. By doping with different alkali metals such as K and Li, similar trend can be found from the O_2-TPD profiles and the "locking-effect" of Li is the smallest among them with the same doping amount. Basically, there are two kinds of Co ions in pure Co_3O_4 crystal structure, tetrahedrally coordinated Co^{2+} and octahedrally coordinated Co^{3+}. For catalytic oxidation applications, octahedrally coordinated Co^{3+} is more active than tetrahedrally coordinated Co^{2+} which has been confirmed by other reports [10,17,24,49,51]. When the alkali metal ions are inserted into the lattice of Co_3O_4, the difference in ionic radii between the alkali metal ions (Li^+ = 0.076 nm, Na^+ = 0.102 nm, K^+ = 0.138 nm) and the cobalt ions (Co^{2+} = 0.078 nm, and Co^{3+} = 0.064 nm), brings about the lattice deformation of Co_3O_4, which will slightly cause the dislocations and imperfections in the spinel crystal structure. But these dislocations and imperfections haven't been observed directly in XRD

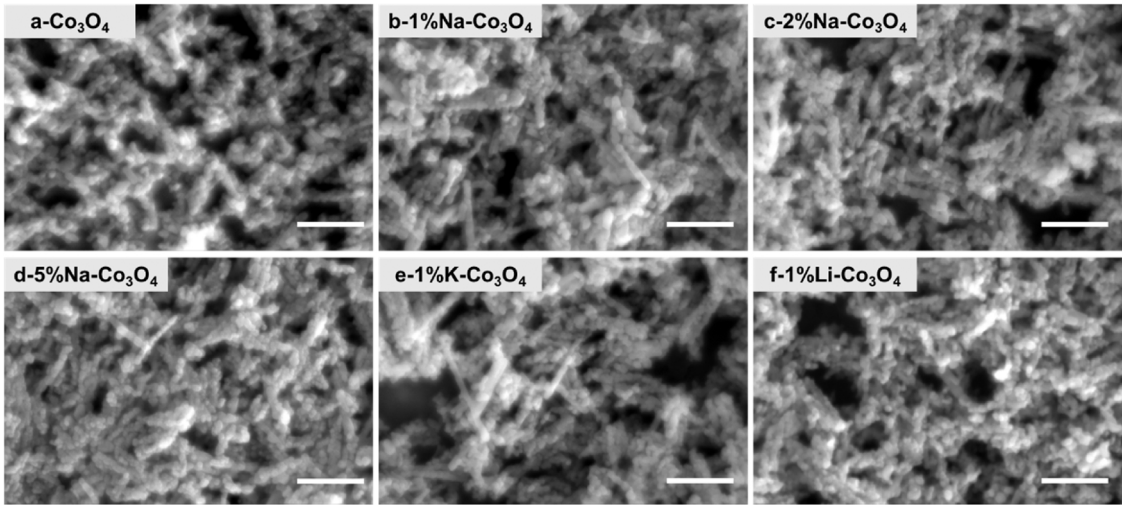

Fig. 7. SEM images of (a) pure Co_3O_4 and (b–f) alkali metal doped Co_3O_4 catalysts (Scale bars: 500 nm).

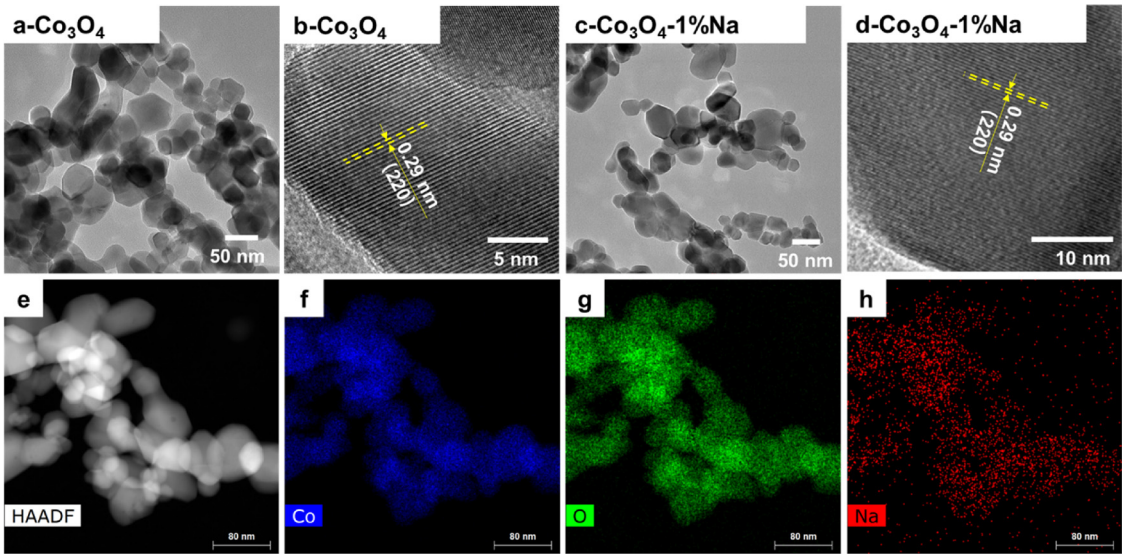

Fig. 8. TEM images of (a and b) pure Co_3O_4 and (c and d)1% Na doped Co_3O_4 catalysts; (e) HAADF-STEM image and (f–h) elemental mapping of 1% Na doped Co_3O_4 catalysts.

spectra with peaks shift, which were similar to *other reports* [52–54]. In case of K doped Co_3O_4, Shang et al. [53] thought that the residual K species was most likely located at the surface and/or in the subsurface layers of Co_3O_4, although it has been proven that parts of K could enter the crystal lattice of Co_3O_4 in K-Co_3O_4 binary catalysts [54]. Herein, there might be two reasons for no peak shift in XRD for the lattice dislocations: one is the lower loading ratio of alkali metals we used, and the degree of lattice dislocation made by alkali metals doping is too small to be observed in XRD spectra; another reason is the alkali metals might concentrate on the surface and subsurface of Co_3O_4 and the main spinel phase of Co_3O_4 was not affected significantly. However, it looks like that these kind of lattice dislocations and imperfections significantly reduce the mobility of surface oxygen due to the existing alkali metal enhance the Co-O bond in doped Co_3O_4. Moreover, due to the similar size of Li^+(0.076 nm), Co^{2+} (0.078 nm) and Co^{3+} (0.064 nm), the doped Li + will have much less effect on the original structure of Co_3O_4, which is in good agreement with the catalytic activity and O_2-TPD results shown before.

Regarding to the surface acid and basic properties, NH_3-TPD and CO_2-TPD analysis were carried out on pure Co_3O_4 and typical 5%Na poisoned Co_3O_4 samples while the results are shown in Fig. 10. Characteristically, two desorption peaks were observed at 100–200 and 300–500 °C over the pure Co_3O_4, which can be ascribed to the weak and strong adsorption of ammonia on the catalyst, separately. It is true that more acid sites will be more beneficial in catalytic reactions like VOCs oxidation [55,56] and NH_3-SCR [57]. With adding Na into the Co_3O_4 catalyst, the temperature peak of NH_3-TPD was shifted to higher temperature with smaller peak area, indicating the acid sites especially at lower temperature have been prohibited significantly, which will further affect the catalytic activities. For CO_2-TPD, the desorption peaks at ca. 80–150 °C, 150–350 °C, and > 550 °C are ascribed to CO_2 adsorbed at weak, medium and strong catalyst basic sites, respectively [53,58].

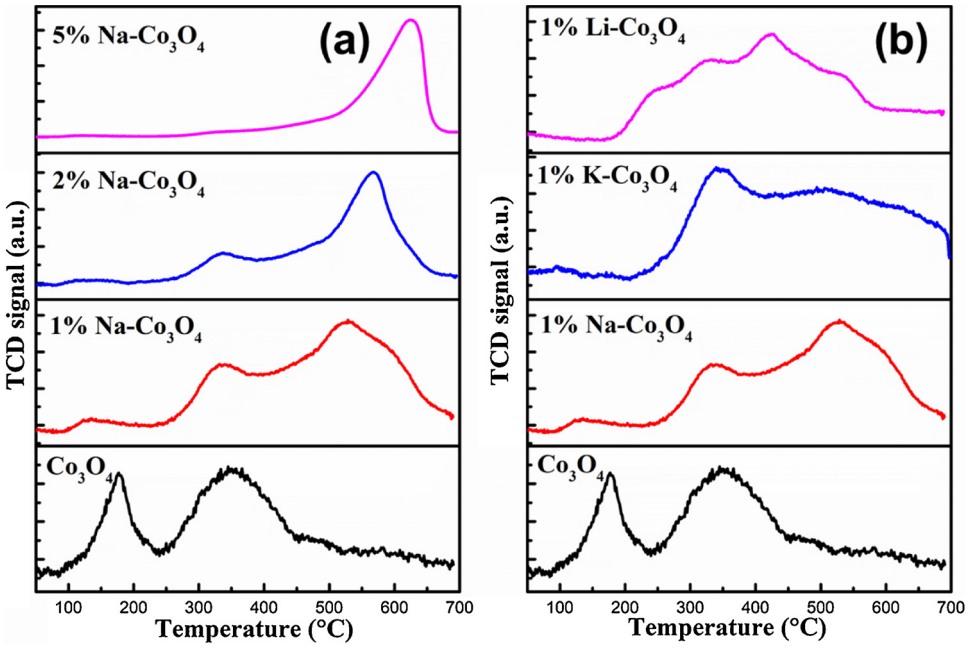

Fig. 9. O_2-TPD profiles of pure Co_3O_4 and alkali metal doped Co_3O_4 catalysts.

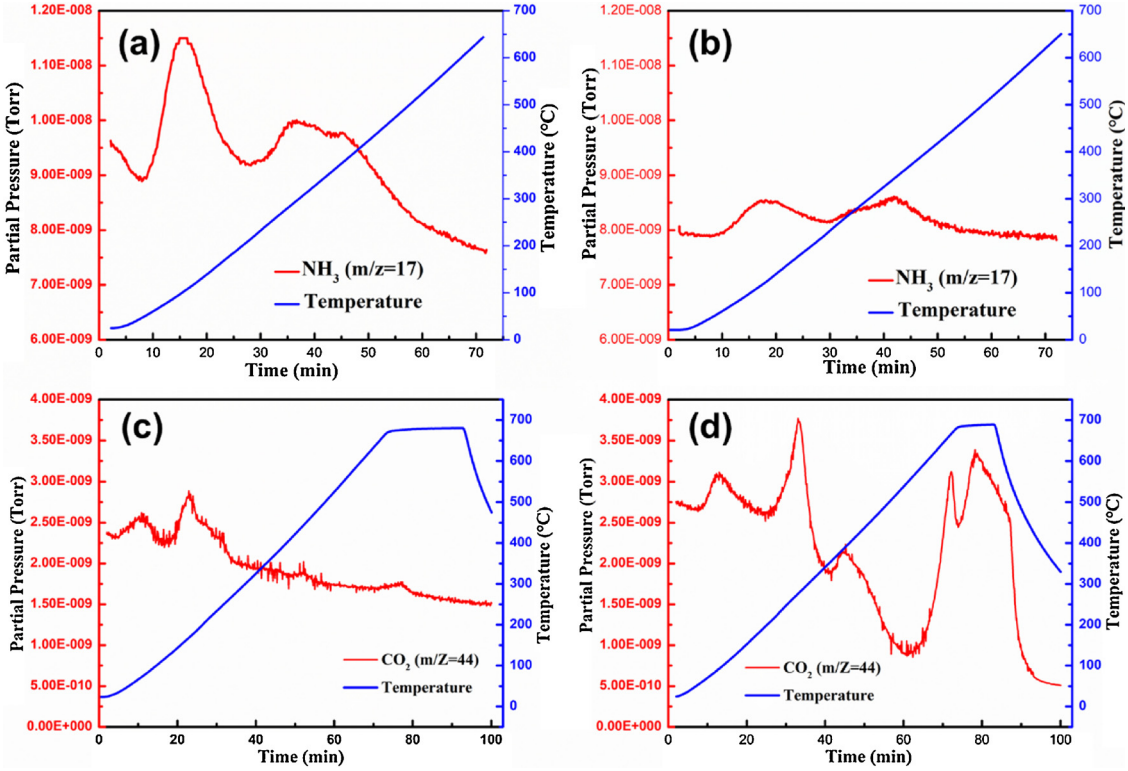

Fig. 10. (a) and (b) NH_3-TPD, (c) and (d) CO_2-TPD profiles of pure Co_3O_4 and 5%-Co_3O_4 catalysts.

With Na doping, the amounts of medium basic sites were significantly increased, indicating that the deposited Na onto Co_3O_4 could vary the surface basicity and electronic properties. It is worth noting that a large amount of CO_2 was desorbed above 500 °C, suggesting CO_2 can adsorb on the surface of Na-doped Co_3O_4 at lower temperature and further generate highly stable carbonate species. This was also confirmed by *in situ* FTIR results and could be an important reason for the poisoning effect.

Fig. 11 shows the CO-TPR results of pure Co_3O_4 and alkali metal doped Co_3O_4 catalysts with detecting the concentration of CO and CO_2 simultaneously. For all profiles, the consumption of CO and formation of CO_2 matches perfectly, indicating all consumed CO molecules were converted to CO_2 with the oxygen species of catalyst. Over the pure Co_3O_4, a small peak centered at 280 °C and a strong peak with shoulder at 313 °C can be assigned to the reduction of Co^{3+} to Co^{2+} and Co^{2+} to Co^0, respectively [59,60]. With alkali metals doping, both reduction peaks were shifted to higher temperature and the area of reduction peak at lower temperature became smaller, indicating the alkali metal has a clearly negative effect on the reducibility of Co_3O_4. The activity of surface oxygen species is regarding as playing a vital role in the catalytic reactions. Therefore, the shift of reduction peak to higher temperature means the less active oxygen species on the alkali metal doped

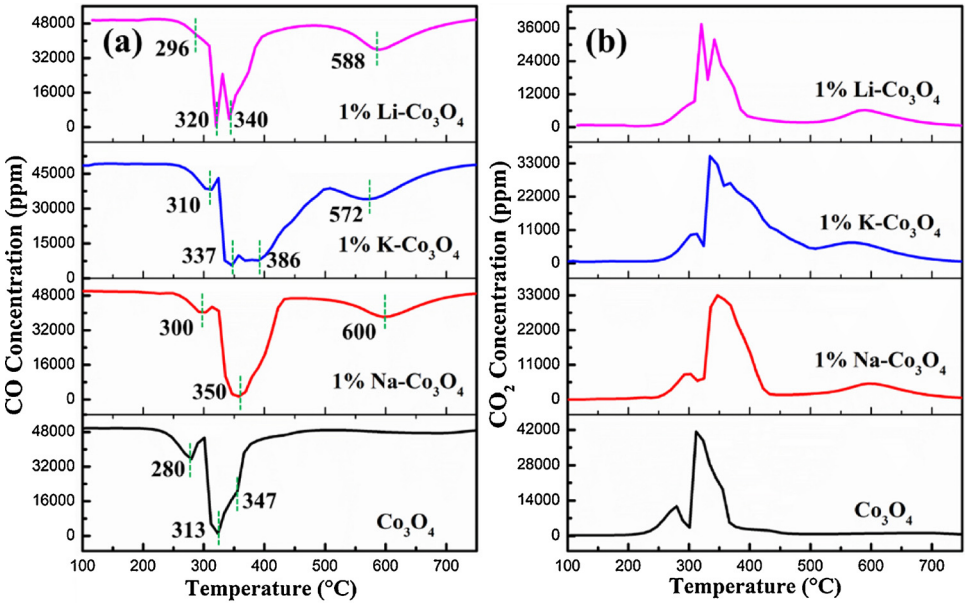

Fig. 11. CO-TPR profiles of pure Co_3O_4 and alkali metal doped Co_3O_4 catalysts (a) CO consumption signal and (b) CO_2 formation signal.

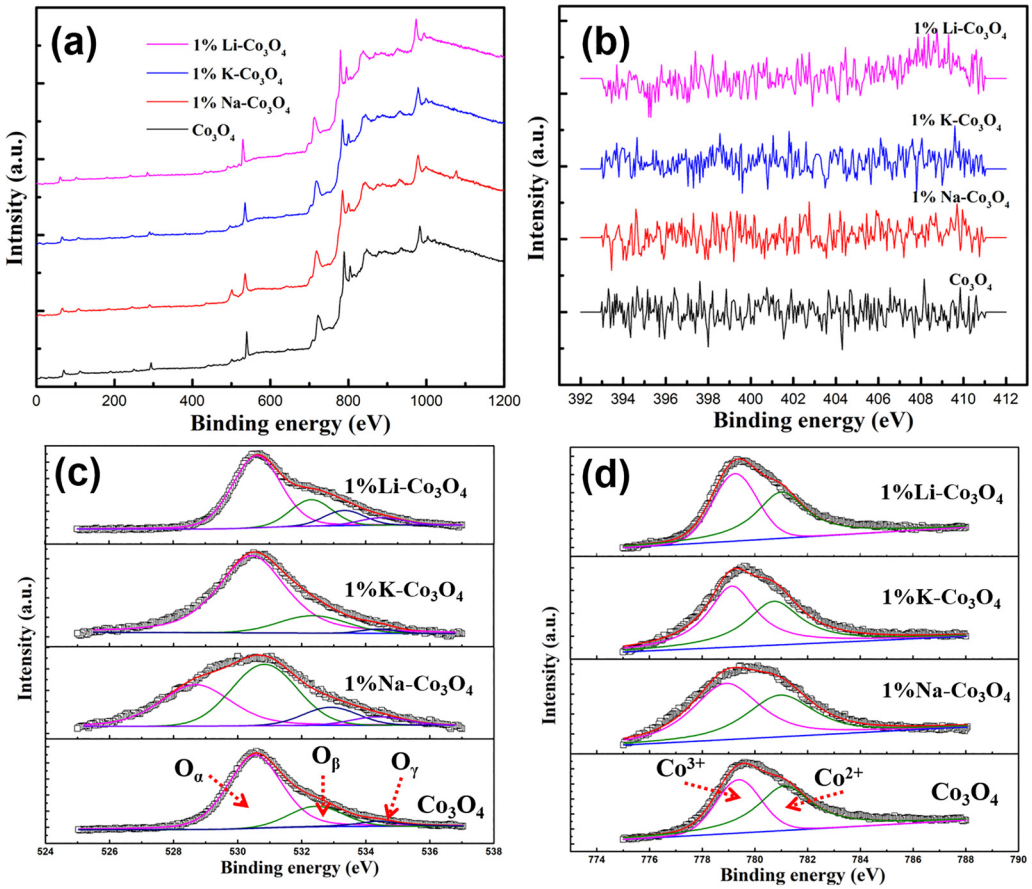

Fig. 12. XPS spectra of Co_3O_4-original and Co_3O_4-AC catalysts: (a) Full spectrum; (b) N1s; (c) O 1s; (d) Co 2p3/2.

samples. Moreover, an additional reduction peak at around 600 °C can be seen on all alkali metal doped samples, which was not observed on the pure Co_3O_4 sample, further indicating a certain amount of oxygen species has been locked (or stabilized) by the doped alkali metals.

Fig. 12a shows the full XPS spectrum of the pure and alkali metals doped Co_3O_4 which confirms the presence of Co, O and alkali metal in related samples. From Fig. 12b, it can be seen that there is no obvious N1 s signal over all samples, indicating the nitrate precursors used in the synthesis decomposed completely and converted into other compounds. With a deconvoluting method (XPSPEAK 4.1), high-resolution Co 2p3/2 and O1 s spectral regions of pure and alkali metal doped samples could be fitted with a few components as shown in Fig. 12c and d, respectively. For example, the Co 2p3/2 peak can be deconvoluted into two parts: lower binding energy at 779.0 ± 0.2 eV and higher binding energy at 780.8 ± 0.2 eV, which can be assigned to the surface Co^{3+} and Co^{2+} species, respectively [10,12,18,61]. The results showed that the Co^{2+}/Co^{3+} ratio of pure Co_3O_4 is 1.48, while the values decreased significantly to 0.76, 0.83, 1.13 for 1%Na, 1%K, 1%Li doped Co_3O_4, respectively. Therefore, the reduction of active Co^{2+} would be an important reason for the poisoning effect of alkali metals. Using similar deconvoluting method, three or four components can be used to fit asymmetrical O1 s peak: lattice oxygen (O_α: O^{2-}) at about 528.7 or 530.5 eV; chemisorbed oxygen species (O_β: O_2^-, O^- and O_2^{2-}) at 532.5 eV; and adsorbed molecular water or hydroxyl group at 534.4 eV (O_γ), as displayed in Fig. 12c. It is well known that the chemisorbed oxygen species on the oxide catalysts has better activities in oxidation reactions. As a result, the ratio of O_β is about 18.9%, while the ratios were 11.1, 15.0 and 18.8% after doping with Na, K, and Li, respectively. The significant decrease of O_β over Na nd K doped samples further confirmed the oxygen activities are restricted by the doping of alkali metals. For the case of Li doped sample, the higher content of O_β might be due to the residual Li_2CO_3 and LiOH formed during the decomposition process.

3.6. *In situ* DRIFT study of CO and C_3H_8 oxidations

An *in situ* DRIFTS study was employed during CO and propane oxidation to further investigate the reactions over the pure Co_3O_4 and 5% Na doped Co_3O_4 catalyst surfaces and to understand the possible poisoning mechanism. The DRIFT spectra of the samples Co_3O_4 and 5% Na doped Co_3O_4 are displayed in Fig. 13, as recorded during the exposure to CO + O_2 with ramping temperature. Over the pure Co_3O_4 catalyst, the bands centering around 1282, 1375 and 1560 cm^{-1} after the sample was heated above 50 °C in CO + O_2 atmosphere can be assigned to bidentate carbonate species [10,19,23,49,62], indicating the occurring of CO oxidation. With looking into the gas-phase bands of CO at around 2116 and 2175 cm^{-1}, we can know that the CO is fully converted at above 130 °C which is in good agreement with the light-off curve achieved before. On the other hand, the bands of bidentate carbonate species firstly became stronger with developed CO conversion along the increasing temperature while disappeared later at above 230 °C with complete CO conversion. At low temperature from 30 to 70 °C, a typical peak at 2056 cm^{-1} can be observed clearly over both pure Co_3O_4 and 5% Na doped Co_3O_4 catalysts, which is attributed to interaction between carbon monoxide and metal sites like CO-Co^{n+} [23,62]. With increasing temperature, this peak vanished at the same time the bands of carbonate species come out, indicating the formation of CO_2 adsorbed on catalyst surface will have a negative effect on the interaction between carbon monoxide and metal sites. Interestingly, the bands of CO-Co^{n+} over 5% Na doped Co_3O_4 catalyst shows much higher intensity than that of pure sample, indicating Na doping significantly promote the CO adsorption strength. Some research has

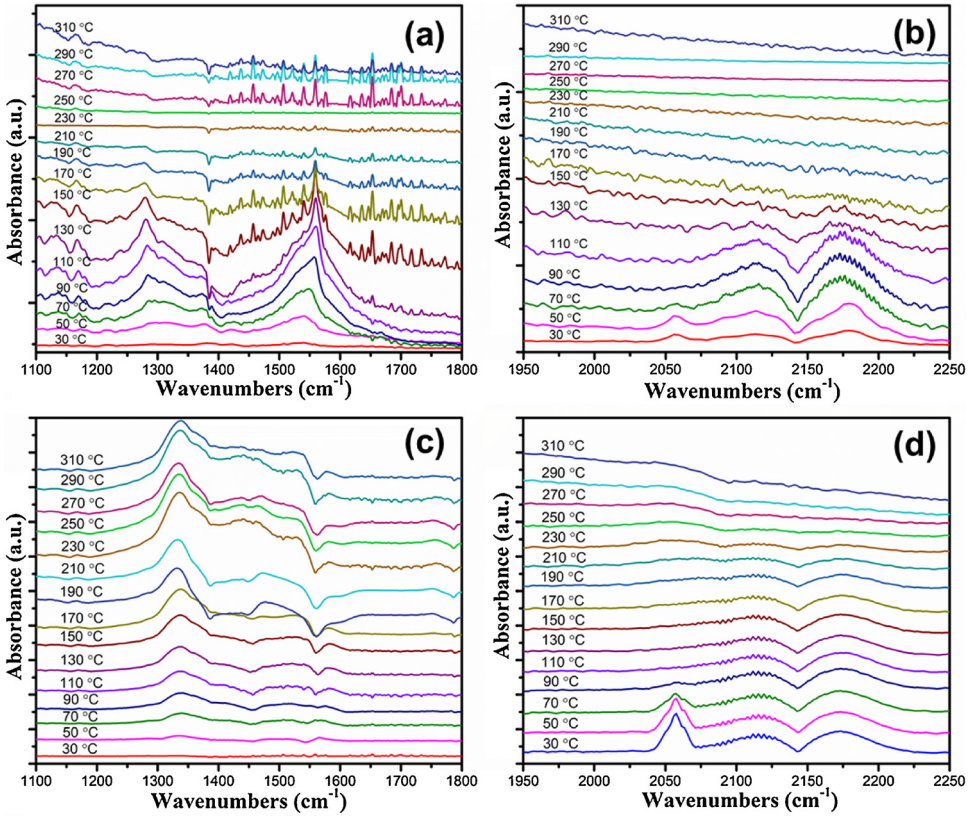

Fig. 13. *In situ* DRIFT spectra recorded for comparison during CO oxidation profiles over pure Co_3O_4 (a and b) and 5%Na doped Co_3O_4 catalysts (c and d).

revealed that strong adsorption of CO would cause higher reaction barrier and strong adsorption of CO_2 could greatly enhance accumulation of surface carbonate species [63–66], then leading to poor activity in CO oxidation. For 5% Na doped Co_3O_4 sample, the bands related to bidentate carbonate species at 1335, 1471, 1537, 1578 cm^{-1} show up above 50 °C after introducing CO + O_2 atmosphere, which are differed from the observation on pure Co_3O_4 sample. These bands become stronger with increasing temperature, demonstrating the accumulation of carbonate species on catalyst surface. It is noteworthy that the carbonate species remain on the catalyst surface even at 310 °C while the CO is fully converted into CO_2 from the light-off curve. This is a significant difference in the feature of carbonate species on the pure and Na-doped Co_3O_4 catalysts, and the carbonate species can be formed on both catalysts at lower temperature while only Na-doped Co_3O_4 can keep these carbonate species stable at higher temperature. Therefore, it is inferred that the doped Na is able to stabilize carbonate species even at high temperature that might be a reason for lower CO activities of Na doped Co_3O_4 catalysts.

Fig. 14 shows the DRIFTS spectra during propane oxidation with ramping process as the testing program, and each spectrum was collected at the specified temperature (30, 50, 80, 110, 140, 170, 200, 230, 260, 290, 320, 350, 380, 410 °C). Typically, the features from 2840~3050 cm^{-1} can be assigned to asymmetric CH_3 stretching and asymmetric CH_2 stretching from gaseous propane [67,68]. Over the pure Co_3O_4 as shown in Fig. 12b, the peaks from 2840~3050 cm^{-1} began to reduce after 230 °C, indicating the oxidation of propane which is in good agreement with the light-off curve displayed before. However, no clear peaks around 1100-1700 cm^{-1} about carbonate species were observed even the propane has already been converted to CO_2 at higher temperature, which tells that the formed CO_2 can immediately desorb on the surface with little further adsorption. In terms of the 5% Na doped Co_3O_4 catalyst, the peak bands about gaseous hydrocarbon still kept very strong even at 410 °C, further confirming the poor activity of propane oxidation. It is evident that some carbonate species with bands around 1367 cm^{-1} [10,23] appear at ~50 °C and accumulation of this kind of species proceeds with the increasing temperature. At the end of propane oxidation over this 5% Na doped Co_3O_4 catalyst, the bands about surface adsorbed carbonate species has the highest intensity although the conversion of propane is still low. With these results, we can deduce that the doped Na has a significantly positive effect on both forming and stabilizing carbonate species on the catalyst surface. Moreover, the carbonate species locked by Na on the surface keep very stable even at temperature as high as 410 °C, which might explain the still poor light-off activity even with the further increased reaction temperature.

3.7. Poisoning mechanism

For the past few years, many researches proposed the CO oxidation reaction on transitional metal oxides followed the Mars-van-Krevelen mechanism [19,22–24,29,64,69] as shown in Fig. 15a. Specifically, CO firstly adsorbed on the cationic metal sites (mostly Co^{3+}); the adsorbed CO reacts with an oxygen atom linked to the active cationic metal sites; CO_2 is formed and desorbs, then oxygen vacancies are generated; oxygen vacancies are filled with gas-phase O_2 to regenerate active oxygen species. As a typical metal oxide, Co_3O_4 can adsorb CO on the surface even at low temperature as confirmed by the strong adsorption peak at 2056 cm^{-1} in previous DRIFT study. With Na doping, this strong Co − CO interaction becomes stronger, indicating the doped Na can significantly promote the CO adsorption strength on cationic metal sites. However, this interaction would be replaced with CO_2 adsorption when the CO_2 is formed by CO oxidation, which can be observed by the DRIFT study. Therefore, the stronger adsorption of CO also means the stronger adsorption of CO_2 [63,64]. It is noted that the stronger adsorption of CO_2 could greatly enhance accumulation of surface carbonate species, then inhibit the CO oxidation. Previous DRFIT study has revealed that the surface carbonate species can be desorbed with increasing temperature on pure Co_3O_4 surface, while this process will be

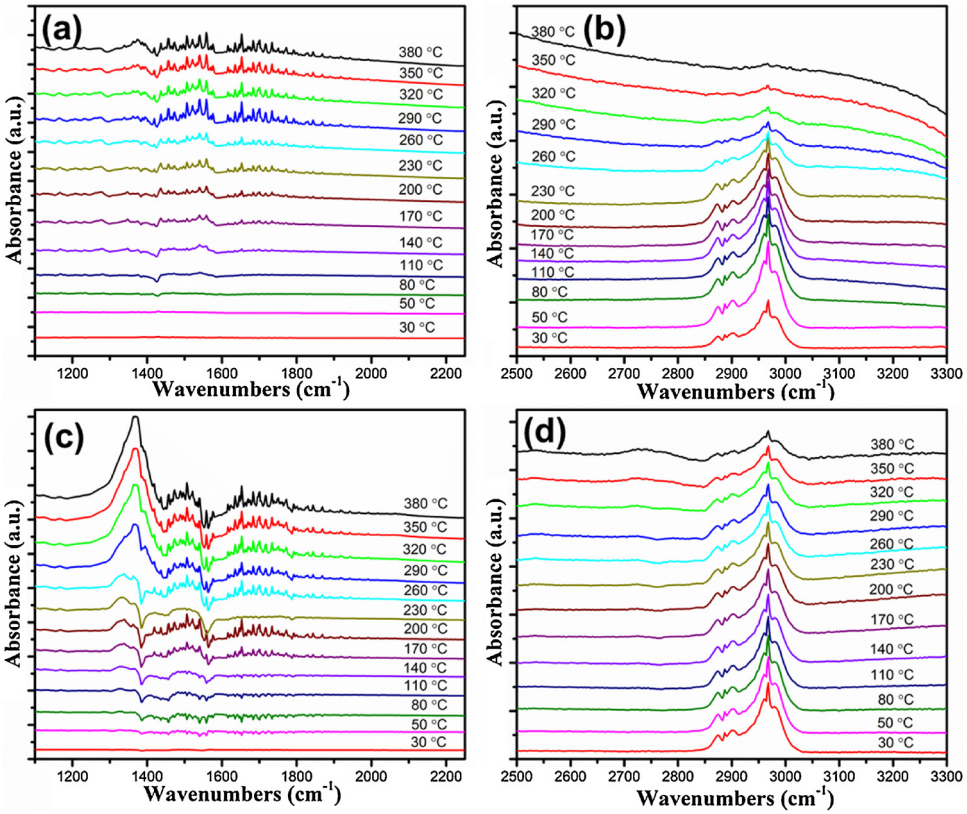

Fig. 14. *In situ* DRIFT spectra recorded for comparison during propane oxidation profiles over pure Co_3O_4 (a and b) and 5% Na doped Co_3O_4 catalysts (c and d).

hard to proceed over the Na doped sample even above 380 °C, while the desorption of highly stable carbonate was observed at temperatures above 500 °C based on the CO_2-TPD results. Moreover, oxygen mobility is also crucial for catalytic oxidation reaction on metal oxides catalysts. Compared to the pure Co_3O_4, doping alkali metal has negative effect on the oxygen mobility of catalyst. From O_2-TPD results, it can be seen that the oxygen desorption shifts to higher temperature obviously with increasing doping amount of Na. The similar results are also observed on other alkali metals dopants such as K and Li.

Based on these results, we can conclude that the poisoning effects of alkali metal doping on Co_3O_4 catalysts in oxidation reactions include: firstly, Na doping would greatly affect the oxygen mobility of Co_3O_4

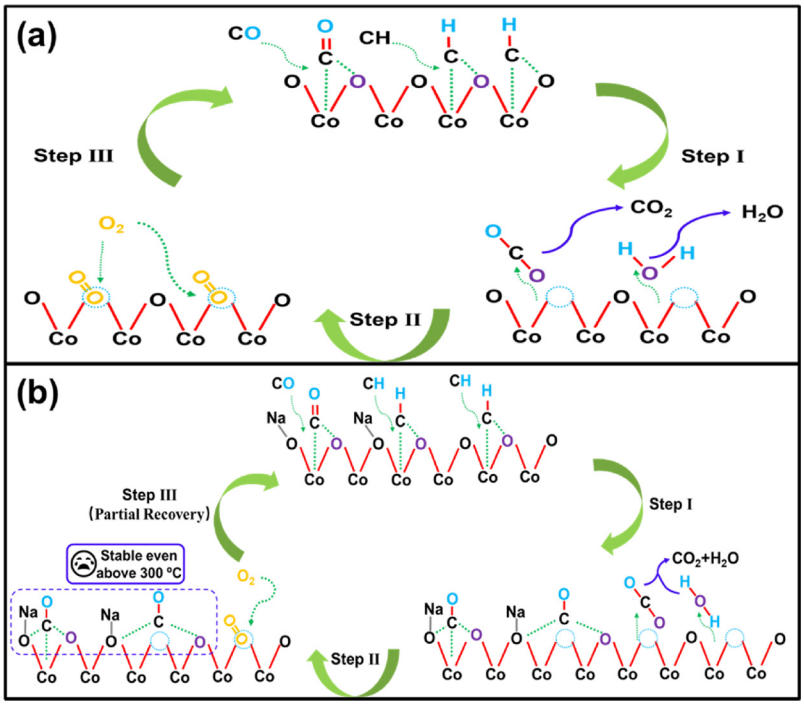

Fig. 15. Schematic models for CO/HC oxidation over (a) pure Co_3O_4 and (b) Na doped Co_3O_4 catalysts.

such as locking oxygen from desorption at low temperature, which makes the catalyst inactive especially at low temperature; Na doping can enhance both CO and CO_2 adsorption on Co_3O_4 surface while the deactivation due to accumulation of surface carbonate species would become severe even at high temperature (a schematic model is shown in Fig. 15b), which will lead to high reaction barrier and poor activity. The similar deactivation mechanism by accumulation of surface carbonate species can be also applied in propane oxidation, which is also demonstrated by the DRIFT study intruded earlier. Besides, this mechanism also explains the reason why high concentration of CO_2 has slight effect on the activity of pure Co_3O_4 catalyst while it has seriously negative effect on the Na-doped Co_3O_4 catalyst even worse than SO_2.

4. Conclusions

Based on this study, one can conclude that deposition of alkali metals can poison the Co_3O_4 catalyst for catalytic oxidation reactions such as CO and propane oxidation, and the Na ions exhibit greater poisoning effect than both Li and K ions. In detail, 1% doping onto Co_3O_4 could increase the light-off temperature by 50 °C in CO oxidation and over 160 °C in propane oxidation, respectively. O_2-TPD results show that alkali metals make a great contribution on the poor oxygen mobility of alkali metal doped catalysts, directly leading the poor oxidation activities. From in-situ DRIFT study, alkali metals can also significantly promote the adsorption of CO_2 to form robust surface carbonate species even at high temperature, another reason for the poisoning effect of alkali metals on Co_3O_4 nanocatalysts for catalytic oxidation, which also explains the worse poisoning effect of high concentration of CO_2 on propane oxidation activity over the Na doped Co_3O_4 catalyst. Our findings about poisoning effect of alkali metals on this highly important oxidation catalyst will give a clear guide for future application of these potential oxidation catalysts. The proposed alkali metal poisoning mechanism could be relevant to the doped Co_3O_4 and other metal oxide oxidation catalysts as well.

Acknowledgements

The authors are grateful for the financial support from the US Department of Energy (Award No. DE-EE0006854) and the US National Science Foundation (Award No. CBET1344792). The research was in part carried out at the Center for Functional Nanomaterials (CFN), Brookhaven National Laboratory (BNL), which is supported by the U.S. Department of Energy, Office of Basic Energy Sciences, under Contract No. DE-SC0012704. The author J.F. Weng is partially supported by a ThermoFisher Scientific Graduate Fellowship. The SEM and partial TEM studies were performed using the facilities in the UConn/ThermoFisher Scientific Center for Advanced Microscopy and Materials Analysis (CAMMA).

References

[1] H. Huang, Y. Xu, Q. Feng, D.Y. Leung, Low temperature catalytic oxidation of volatile organic compounds: a review, Catal. Sci. Technol. 5 (2015) 2649–2669.
[2] H. Xu, N. Yan, Z. Qu, W. Liu, J. Mei, W. Huang, S. Zhao, Gaseous Heterogeneous Catalytic Reactions over Mn-Based Oxides for Environmental Applications: a Critical Review, Environ. Sci. Technol. 51 (2017) 8879–8892.
[3] M.S. Kamal, S.A. Razzak, M.M. Hossain, Catalytic oxidation of volatile organic compounds (VOCs)–areview, Atmos. Environ. 140 (2016) 117–134.
[4] P. Gélin, M. Primet, Complete oxidation of methane at low temperature over noble metal based catalysts: a review, Appl. Catal. B 39 (2002) 1–37.
[5] A. Vazquez, A. Kato, L. Schmidt, Sulfur on noble metal catalyst particles, J. Catal. 78 (1982) 306–318.
[6] H. Gandhi, M. Shelef, Effects of sulphur on noble metal automotive catalysts, Appl. Catal. 77 (1991) 175–186.
[7] S. Royer, D. Duprez, Catalytic oxidation of carbon monoxide over transition metal oxides, ChemCatChem 3 (2011) 24–65.
[8] W. Li, J. Wang, H. Gong, Catalytic combustion of VOCs on non-noble metal catalysts, Catal. Today 148 (2009) 81–87.
[9] W. Tang, W. Xiao, S. Wang, Z. Ren, J. Ding, P.X. Gao, Boosting catalytic propane oxidation over PGM-free Co 3 O 4 nanocrystal aggregates through chemical leaching: a comparative study with Pt and Pd based catalysts, Appl. Catal. B Environ. 226 (2018) 585–595.
[10] Z. Ren, Z. Wu, W. Song, W. Xiao, Y. Guo, J. Ding, S.L. Suib, P.-X. Gao, Low temperature propane oxidation over Co3O4 based nano-array catalysts: Ni dopant effect, reaction mechanism and structural stability, Appl. Catal. B 180 (2016) 150–160.
[11] Z. Ren, Y. Guo, Z. Zhang, C. Liu, P.-X. Gao, Nonprecious catalytic honeycombs structured with three dimensional hierarchical Co 3 O 4 nano-arrays for high performance nitric oxide oxidation, J. Mater. Chem. A 1 (2013) 9897–9906.
[12] B. Bai, H. Arandiyan, J. Li, Comparison of the performance for oxidation of formaldehyde on nano-Co3O4, 2D-Co3O4, and 3D-Co3O4 catalysts, Appl. Catal. B 142–143 (2013) 677–683.
[13] B. Bai, J. Li, Positive effects of K+ ions on three-dimensional mesoporous Ag/Co3O4 catalyst for HCHO oxidation, ACS Catal. 4 (2014) 2753–2762.
[14] M. Dhakad, T. Mitshuhashi, S. Rayalu, P. Doggali, S. Bakardjiva, J. Subrt, D. Fino, H. Haneda, N. Labhsetwar, Co3O4–CeO2 mixed oxide-based catalytic materials for diesel soot oxidation, Catal. Today 132 (2008) 188–193.
[15] M.F. Irfan, J.H. Goo, S.D. Kim, Co3O4 based catalysts for NO oxidation and NOx reduction in fast SCR process, Appl. Catal. B 78 (2008) 267–274.
[16] B. Meng, Z. Zhao, X. Wang, J. Liang, J. Qiu, Selective catalytic reduction of nitrogen oxides by ammonia over Co3O4 nanocrystals with different shapes, Appl. Catal. B 129 (2013) 491–500.
[17] X. Xie, Y. Li, Z.-Q. Liu, M. Haruta, W. Shen, Low-temperature oxidation of CO catalysed by Co3O4 nanorods, Nature 458 (2009) 746–749.
[18] Z. Zhu, G. Lu, Z. Zhang, Y. Guo, Y. Guo, Y. Wang, Highly active and stable Co3O4/ZSM-5 catalyst for propane oxidation: effect of the preparation method, ACS Catal. 3 (2013) 1154–1164.
[19] J.-Y. Luo, M. Meng, Y.-Q. Zha, L.-H. Guo, Identification of the active sites for CO and C3H8 total oxidation over nanostructured CuO− CeO2 and Co3O4− CeO2 catalysts, J. Phys. Chem. C 112 (2008) 8694–8701.
[20] A.J. Binder, T.J. Toops, R.R. Unocic, J.E. Parks, S. Dai, Low-temperature CO oxidation over a ternary oxide catalyst with high resistance to hydrocarbon inhibition, Angew. Chemie Int. Ed. 54 (2015) 13263–13267.
[21] L. Liotta, G. Di Carlo, G. Pantaleo, G. Deganello, Catalytic performance of Co3O4/CeO2 and Co3O4/CeO2–ZrO2 composite oxides for methane combustion: influence of catalyst pretreatment temperature and oxygen concentration in the reaction mixture, Appl. Catal. B 70 (2007) 314–322.
[22] Y. Lou, L. Wang, Z. Zhao, Y. Zhang, Z. Zhang, G. Lu, Y. Guo, Y. Guo, Low-temperature CO oxidation over Co3O4-based catalysts: significant promoting effect of Bi2O3 on Co3O4 catalyst, Appl. Catal. B 146 (2014) 43–49.
[23] Z. Liu, Z. Wu, X. Peng, A. Binder, S. Chai, S. Dai, Origin of active oxygen in a ternary CuO x/Co3O4–CeO2 catalyst for CO oxidation, J. Phys. Chem. C 118 (2014) 27870–27877.
[24] Y. Lou, J. Ma, X. Cao, L. Wang, Q. Dai, Z. Zhao, Y. Cai, W. Zhan, Y. Guo, P. Hu, Promoting effects of In2O3 on Co3O4 for CO oxidation: tuning O2 activation and CO adsorption strength simultaneously, ACS Catal. 4 (2014) 4143–4152.
[25] W. Tang, Y. Deng, W. Li, S. Li, X. Wu, Y. Chen, Restrictive nanoreactor for growth of transition metal oxides (MnO2, Co3O4, NiO) nanocrystal with enhanced catalytic oxidation activity, Catal. Commun. 72 (2015) 165–169.
[26] L. Liotta, M. Ousmane, G. Di Carlo, G. Pantaleo, G. Deganello, G. Marcì, L. Retailleau, A. Giroir-Fendler, Total oxidation of propene at low temperature over Co3O4–CeO2 mixed oxides: role of surface oxygen vacancies and bulk oxygen mobility in the catalytic activity, Appl. Catal. A Gen. 347 (2008) 81–88.
[27] Y. Peng, J. Li, L. Chen, J. Chen, J. Han, H. Zhang, W. Han1, Alkali metal poisoning of a CeO2–WO3 catalyst used in the selective catalytic reduction of NO x with NH3: an experimental and theoretical study, Environ. Sci. Technol. 46 (2012) 2864–2869.
[28] O. Kroecher, M. Elsener, Chemical deactivation of V2O5/WO3–TiO2 SCR catalysts by additives and impurities from fuels, lubrication oils, and urea solution: I. Catalytic studies, Appl. Catal. B 77 (2008) 215–227.
[29] J.-Y. Luo, M. Meng, X. Li, X.G. Li, Y.-Q. Zha, T.-D. Hu, Y.-N. Xie, J. Zhang, Mesoporous Co3O4–CeO2 and Pd/Co3O4–CeO2 catalysts: synthesis, characterization and mechanistic study of their catalytic properties for low-temperature CO oxidation, J. Catal. 254 (2008) 310–324.
[30] Y. Peng, J. Li, W. Si, J. Luo, Y. Wang, J. Fu, X. Li, J. Crittenden, J. Hao, Deactivation and regeneration of a commercial SCR catalyst: comparison with alkali metals and arsenic, Appl. Catal. B 168 (2015) 195–202.
[31] Y. Peng, J. Li, X. Huang, X. Li, W. Su, X. Sun, D. Wang, J. Hao, Deactivation mechanism of potassium on the V2O5/CeO2 catalysts for SCR reaction: acidity, reducibility and adsorbed-NO x, Environ. Sci. Technol. 48 (2014) 4515–4520.
[32] F. Tang, B. Xu, H. Shi, J. Qiu, Y. Fan, The poisoning effect of Na+ and Ca2+ ions doped on the V2O5/TiO2 catalysts for selective catalytic reduction of NO by NH3, Appl. Catal. B 94 (2010) 71–76.
[33] C. Zhang, F. Liu, Y. Zhai, H. Ariga, N. Yi, Y. Liu, K. Asakura, M. Flytzani-Stephanopoulos, H. He, Alkali-metal-Promoted Pt/TiO2 opens a more efficient pathway to formaldehyde oxidation at ambient temperatures, Angew. Chemie Int. Ed. 51 (2012) 9628–9632.
[34] E. Aneggi, C. de Leitenburg, G. Dolcetti, A. Trovarelli, Diesel soot combustion activity of ceria promoted with alkali metals, Catal. Today 136 (2008) 3–10.
[35] H. An, P.J. McGinn, Catalytic behavior of potassium containing compounds for diesel soot combustion, Appl. Catal. B 62 (2006) 46–56.
[36] A.A. Mirzaei, H.R. Shaterian, R.W. Joyner, M. Stockenhuber, S.H. Taylor, G.J. Hutchings, Ambient temperature carbon monoxide oxidation using copper manganese oxide catalysts: effect of residual Na+ acting as catalyst poison, Catal. Commun. 4 (2003) 17–20.
[37] M. Haneda, Y. Kintaichi, N. Bion, H. Hamada, Alkali metal-doped cobalt oxide

catalysts for NO decomposition, Appl. Catal. B 46 (2003) 473–482.
[38] K. Asano, C. Ohnishi, S. Iwamoto, Y. Shioya, M. Inoue, Potassium-doped Co3O4 catalyst for direct decomposition of N2O, Appl. Catal. B 78 (2008) 242–249.
[39] Q. Yan, X. Li, Q. Zhao, G. Chen, Shape-controlled fabrication of the porous Co3O4 nanoflower clusters for efficient catalytic oxidation of gaseous toluene, J. Hazard. Mater. 209 (2012) 385–391.
[40] T. Zeng, X. Zhang, S. Wang, H. Niu, Y. Cai, Spatial confinement of a Co3O4 catalyst in hollow metal–Organic frameworks as a nanoreactor for improved degradation of organic pollutants, Environ. Sci. Technol. 49 (2015) 2350–2357.
[41] M. Brooker, J.B. Bates, Raman and infrared spectral studies of anhydrous Li2CO3 and Na2CO3, J. Chem. Phys. 54 (1971) 4788–4796.
[42] W. Simanjuntak, S. Sembiring, W.A. Zakaria, K.D. Pandiangan, The use of carbon dioxide released from coconut shell combustion to produce Na2CO3, Makara J. Sci. (2014) 65–70.
[43] M. Sulaiman, N. Dzulkarnain, A. Rahman, N. Mohamed, Sol–gel synthesis and characterization of LiNO3–Al2O3 composite solid electrolyte, Solid State Sci. 14 (2012) 127–132.
[44] H. Song, U.S. Ozkan, Ethanol steam reforming over Co-based catalysts: role of oxygen mobility, J. Catal. 261 (2009) 66–74.
[45] W. Si, Y. Wang, S. Zhao, F. Hu, J. Li, A facile method for in situ preparation of the MnO2/LaMnO3 catalyst for the removal of toluene, Environ. Sci. Technol. 50 (2016) 4572–4578.
[46] S. Royer, D. Duprez, S. Kaliaguine, Role of bulk and grain boundary oxygen mobility in the catalytic oxidation activity of LaCo1–xFexO3, J. Catal. 234 (2005) 364–375.
[47] J. KT, Thermodynamics of cobalt (II, III) oxide (Co3O4): evidence of phase transition, Trans. Jpn. Inst. Met. 29 (1988) 125–132.
[48] M. Alifanti, J. Kirchnerova, B. Delmon, D. Klvana, Methane and propane combustion over lanthanum transition-metal perovskites: role of oxygen mobility, Appl. Catal. A Gen. 262 (2004) 167–176.
[49] L. Xue, C. Zhang, H. He, Y. Teraoka, Catalytic decomposition of N2O over CeO2 promoted Co3O4 spinel catalyst, Appl. Catal. B 75 (2007) 167–174.
[50] Y. Yu, T. Takei, H. Ohashi, H. He, X. Zhang, M. Haruta, Pretreatments of Co3O4 at moderate temperature for CO oxidation at –80° C, J. Catal. 267 (2009) 121–128.
[51] M. Zhou, L. Cai, M. Bajdich, M. García-Melchor, H. Li, J. He, J. Wilcox, W. Wu, A. Vojvodic, X. Zheng, Enhancing catalytic CO oxidation over Co3O4 nanowires by substituting Co2+ with Cu2+, ACS Catal. 5 (2015) 4485–4491.
[52] C. Ohnishi, K. Asano, S. Iwamoto, K. Chikama, M. Inoue, Alkali-doped Co3O4 catalysts for direct decomposition of N2O in the presence of oxygen, Catal. Today 120 (2007) 145–150.
[53] Z. Shang, M. Sun, X. Che, W. Wang, L. Wang, X. Cao, W. Zhan, Y. Guo, Y. Guo, G. Lu, The existing states of potassium species in K-doped Co 3 O 4 catalysts and their influence on the activities for NO and soot oxidation, Catal. Sci. Technol. 7 (2017) 4710–4719.
[54] M. Sun, L. Wang, B. Feng, Z. Zhang, G. Lu, Y. Guo, The role of potassium in K/Co3O4 for soot combustion under loose contact, Catal. Today 175 (2011) 100–105.
[55] B. de Rivas, R. López-Fonseca, C. Jiménez-González, J.I. Gutiérrez-Ortiz, Synthesis, characterisation and catalytic performance of nanocrystalline Co3O4 for gas-phase chlorinated VOC abatement, J. Catal. 281 (2011) 88–97.
[56] S. Jiang, S. Song, Enhancing the performance of Co3O4/CNTs for the catalytic combustion of toluene by tuning the surface structures of CNTs, Appl. Catal. B 140 (2013) 1–8.
[57] H. Hu, S. Cai, H. Li, L. Huang, L. Shi, D. Zhang, In situ DRIFTs investigation of the low-temperature reaction mechanism over Mn-Doped Co3O4 for the selective catalytic reduction of NO x with NH3, J. Phys. Chem. C 119 (2015) 22924–22933.
[58] H. Chang, M. Li, Z. Li, L. Duan, C. Zhao, J. Li, J. Hao, Design strategies of surface basicity for NO oxidation over a novel Sn–Co–O catalyst in the presence of H 2 O, Catal. Sci. Technol. 7 (2017) 2057–2064.
[59] L. Hu, K. Sun, Q. Peng, B. Xu, Y. Li, Surface active sites on Co 3 O 4 nanobelt and nanocube model catalysts for CO oxidation, Nano Res. 3 (2010) 363–368.
[60] L. Liotta, G. Di Carlo, G. Pantaleo, G. Deganello, Co3O4/CeO2 and Co3O4/CeO2–ZrO2 composite catalysts for methane combustion: correlation between morphology reduction properties and catalytic activity, Catal. Commun. 6 (2005) 329–336.
[61] B. Bai, J. Li, Positive effects of K+Ions on three-dimensional mesoporous Ag/Co3O4Catalyst for HCHO oxidation, ACS Catal. 4 (2014) 2753–2762.
[62] F. Grillo, M.M. Natile, A. Glisenti, Low temperature oxidation of carbon monoxide: the influence of water and oxygen on the reactivity of a Co3O4 powder surface, Appl. Catal. B 48 (2004) 267–274.
[63] Z.-P. Liu, P. Hu, General trends in the barriers of catalytic reactions on transition metal surfaces, J. Chem. Phys. 115 (2001) 4977–4980.
[64] H.-F. Wang, R. Kavanagh, Y.-L. Guo, Y. Guo, G. Lu, P. Hu, Origin of extraordinarily high catalytic activity of Co3O4 and its morphological chemistry for CO oxidation at low temperature, J. Catal. 296 (2012) 110–119.
[65] H.-K. Lin, C.-B. Wang, H.-C. Chiu, S.-H. Chien, In situ FTIR study of cobalt oxides for the oxidation of carbon monoxide, Catal. Letters 86 (2003) 63–68.
[66] J. Jansson, M. Skoglundh, E. Fridell, P. Thormählen, A mechanistic study of low temperature CO oxidation over cobalt oxide, Top. Catal. 16 (2001) 385–389.
[67] S. Natesakhawat, O. Oktar, U.S. Ozkan, Effect of lanthanide promotion on catalytic performance of sol–gel Ni/Al2O3 catalysts in steam reforming of propane, J. Mol. Catal. A Chem. 241 (2005) 133–146.
[68] A. Hinz, M. Skoglundh, E. Fridell, A. Andersson, An investigation of the reaction mechanism for the promotion of propane oxidation over Pt/Al2O3 by SO2, J. Catal. 201 (2001) 247–257.
[69] J. Jansson, A.E. Palmqvist, E. Fridell, M. Skoglundh, L. Österlund, P. Thormählen, V. Langer, On the catalytic activity of Co3O4 in low-temperature CO oxidation, J. Catal. 211 (2002) 387–397.